Entry Length Requirements for 2D and 3D Laminar Couette-Poiseuille Flows

Bayode E. Owolabi*
Department of Mechanical Engineering
University of Alberta
Edmonton, T6G 1H9, Canada
owolabi@ualberta.ca

David J. C. Dennis
School of Engineering
University of Liverpool
Liverpool, L69 3GH, United Kingdom
djcd@liverpool.ac.uk

Robert J. Poole
School of Engineering
University of Liverpool
Liverpool, L69 3GH, United Kingdom
robpoole@liverpool.ac.uk

ABSTRACT

In this study, we examine the development length requirements for laminar Couette-Poiseuille flows in a two-dimensional (2D) channel as well as in the three-dimensional (3D) case of flow through a square duct, using a combination of numerical and experimental approaches. The parameter space investigated covers wall to bulk velocity ratios, r, spanning from 0 (purely pressure-driven flow) to 2 (purely wall driven-flow; 4 in the case of a square duct) and a wide range of Reynolds numbers (Re). The results indicate an increase in the development length (L) with r. Consistent with the findings of Durst et al. [1], L was observed to be of the order of the channel height in the limit as $Re \to 0$, irrespective of the condition at the inlet. This, however, changes at high Reynolds numbers, with L increasing linearly with Re. In all the cases considered, a uniform velocity profile at the inlet was found to result in longer entry lengths than in a flow developing from a parabolic inlet profile. We show that this inlet effect becomes less important as the limit of purely wall-driven flow is approached. Finally, we develop correlations for predicting L in these flows and, for the

*Address all correspondence to this author.

first time, also present laser Doppler velocimetry (LDV) measurements of the developing as well as fully-developed velocity profiles, and observe good agreement between experiment, analytical solution, and numerical simulation results in the 3D case.

INTRODUCTION

Laminar flow development and entrance effects in ducts have been the subject of extensive research, due to their huge importance in practical applications as well as in fundamental studies on the characteristics of duct flows **[2, 3]**. From a prescribed velocity profile at the inlet, a flow field evolves in the streamwise direction, satisfying the no-slip condition at the walls; boundary layers which grow with distance from the inlet are thus formed. Eventually, these boundary layers coalesce and the velocity profile becomes invariant with streamwise distance, the flow having become "fully developed". The distance from the inlet at which this occurs is referred to as the development or entry length (L). The entrance region is usually associated with a higher pressure drop than in fully developed flow due to the increased shear stress at the wall, hence a knowledge of L is very important in making predictions about skin friction drag and heat transfer.

Although the flow development phenomenon is well understood, it is surprising that correlations which accurately predict the entry length have only been developed fairly recently (see e.g. [1, 4–7]). Using simple scaling arguments, [1] showed the important roles played by both molecular diffusion as well as convection in the flow development process. The former was ignored in most previous studies **(see [1] for a summary of results from previous investigations)**, thus leading to a wide variation in the predicted value of L. For Reynolds numbers, $Re = \rho U_b D/\mu$ (ρ, μ and U_b represent density, dynamic viscosity, bulk velocity and channel height, respectively, while D is the characteristic length scale of a duct, such as the pipe diameter or channel height) tending to zero where diffusion dominates, L/D is essentially a constant, independent of the Reynolds number; however, at $Re \to \infty$, L/D varies linearly with Reynolds number, due to the dominance of convection. Hence an appropriate expression for the development length should be of the form

$$L/D = C_0 + C_1 Re. \tag{1}$$

In turbulent flows, the chaotic mixing by randomly fluctuating eddies causes the effect of molecular diffusion to be overshadowed; therefore, the entry lengths are much smaller than in laminar flow due to the diffusive nature of these eddies [8]. However, it should be noted that most duct flows

(such as those in a pipe or square duct) are linearly stable at all Reynolds numbers [9], hence a laminar flow can, theoretically, be maintained indefinitely. L is thus expected to become very large as $Re \to \infty$. For Laminar flow of a Newtonian fluid in pipes and two-dimensional channels, the following non-linear equations respectively hold [1]

$$L/D = [(0.619)^{\frac{8}{5}} + (0.0567Re)^{\frac{8}{5}}]^{\frac{5}{8}} \tag{2}$$

$$L/D = [(0.631)^{\frac{8}{5}} + (0.0442Re)^{\frac{8}{5}}]^{\frac{5}{8}}. \tag{3}$$

Similar correlations have also been proposed for concentric annuli [4] as well as non-Newtonian flows [5, 6].

Furthermore, there have been studies on the effect of wall slip [10–12], compressibility [13] and sinusoidal pulsations [14] on the development length, and formulations for ducts of different aspect ratios have been given [15]. The focus has been mainly on pressure-driven (Poiseuille) flows, hence wall-driven (Couette) flows will be explored in this study. These are encountered in a wide range of industrial applications such as in cooling systems of rotating machinery [16], filtration devices [17] and catalytic chemical reactors [18] among others. We investigate the combined effects of a pressure gradient and wall translation on the entry lengths in a 2D channel, and extend the results to the 3D case of flow in a square duct. **It is surprising how little data there is in the literature – either numerical or experimental – for Couette-Poiseuille flow in this geometry. Even the laminar analytical solution for fully-developed flow [26] has only been published very recently and this has never been confirmed experimentally. As such, we present the first ever experimental measurements of laminar Couette-Poiseuille flow in a square duct both developing and fully-developed for a number of different conditions. We also provide extensive new numerical simulations for the development length in this set-up**

and obtain simple correlations for estimating the entry length in Couette-Poiseuille flows over the full range of wall-to-bulk velocity ratios, r (spanning from the purely pressure-driven case to purely wall-driven flow).

NUMERICAL SIMULATIONS

The governing transport equations for the Couette-Poiseuille flow problem are those expressing conservation of mass and momentum. For 3D flow, the equations respectively read

$$\frac{\partial u}{\partial x} + \frac{\partial v}{\partial y} + \frac{\partial w}{\partial z} = 0 \tag{4}$$

$$\rho\left(u\frac{\partial u}{\partial x} + v\frac{\partial u}{\partial y} + w\frac{\partial u}{\partial z}\right) = -\frac{\partial p}{\partial x} + \mu\left(\frac{\partial^2 u}{\partial x^2} + \frac{\partial^2 u}{\partial y^2} + \frac{\partial^2 u}{\partial z^2}\right)$$

$$\rho\left(u\frac{\partial v}{\partial x} + v\frac{\partial v}{\partial y} + w\frac{\partial v}{\partial z}\right) = -\frac{\partial p}{\partial y} + \mu\left(\frac{\partial^2 v}{\partial x^2} + \frac{\partial^2 v}{\partial y^2} + \frac{\partial^2 v}{\partial z^2}\right)$$

$$\rho\left(u\frac{\partial w}{\partial x} + v\frac{\partial w}{\partial y} + w\frac{\partial w}{\partial z}\right) = -\frac{\partial p}{\partial z} + \mu\left(\frac{\partial^2 w}{\partial x^2} + \frac{\partial^2 w}{\partial y^2} + \frac{\partial^2 w}{\partial z^2}\right), \tag{5}$$

where x, y and z represent the streamwise, transverse and spanwise co-ordinates, respectively, and u, v and w are the corresponding velocity components. Equations 4 and 5 simplify to the

following in the 2-D channel

$$\frac{\partial u}{\partial x} + \frac{\partial v}{\partial y} = 0 \tag{6}$$

$$\rho\left(u\frac{\partial u}{\partial x} + v\frac{\partial u}{\partial y}\right) = -\frac{\partial p}{\partial x} + \mu\left(\frac{\partial^2 u}{\partial x^2} + \frac{\partial^2 u}{\partial y^2}\right)$$

$$\rho\left(u\frac{\partial v}{\partial x} + v\frac{\partial v}{\partial y}\right) = -\frac{\partial p}{\partial y} + \mu\left(\frac{\partial^2 v}{\partial x^2} + \frac{\partial^2 v}{\partial y^2}\right). \tag{7}$$

In solving the above equations numerically, the commercial software, ANSYS Fluent, was utilised. This package has been extensively used in fluid dynamics research (see e.g. [6, 19–23]). The momentum equations are discretised using the second-order upwind scheme, while coupling between velocity and pressure is implemented using the semi-implicit method for pressure-linked equations (SIMPLE, see [24]).

Figures 1 and 2 show the schematics of the computational domain for the numerical simulations and the co-ordinate systems employed. At the walls, the no slip boundary condition (i.e fluid velocity at the boundary is equal to the wall velocity) is imposed. Two types of inlet boundary conditions are examined. In the first, a uniform velocity profile (most commonly used in research on development length) is applied at the inlet. For this case, the entire top wall is made to translate (see Figs. 1a and 2a). In the second case, a parabolic velocity profile (corresponding to that of the fully-developed pressure-driven flow at a given bulk velocity) is introduced at the inlet (see Figs. 1b and 2b), and wall motion is imposed only after a streamwise distance of a few duct heights (D) from the inlet. This position is taken as the $x = 0$ location (in the previous case, $x = 0$ is located

at the duct inlet). The wall motion is terminated at a few Ds from the outlet to match the configuration of the experimental setup which will be described in the section on experimental studies. In all cases, zero axial gradients are imposed at the outlet and the length of the moving-wall region was set to be a function of the Reynolds number, at least three times as long as the development length being computed. Computations on longer domains yielded identical results to those based on the above criterion, thus indicating that the solutions obtained are independent of the domain length.

By convention, the development length is usually defined as the axial distance from the $x = 0$ location, for the maximum velocity, u_{max}, to monotonically [1] attain a value which is within one percent of its fully developed analytical value. The choice of 1% is rather arbitrary as the exact fully developed value is approached asymptotically. For a purely pressure-driven flow developing from a uniform velocity profile at the inlet, u_{max} corresponds to the centreline velocity. However, in Couette-Poiseuille flows, the wall-normal location of u_{max} is shifted towards the moving wall as r increases. In the limiting case of purely wall-driven flow, the peak velocity is located at the moving wall. The flow at this location instantaneously becomes fully developed as a result of the no-slip condition, hence in calculating the development length for this case, it is more appropriate to examine the entire velocity profile. In this study, a comparison between the entry length values obtained using both the local (based on u_{max} location) and global (based on entire velocity profile) criteria is made.

The laminar flow analytical solutions for fully-developed 2D Couette-Poiseuille flow [25] is given by

$$u = \frac{1}{2\mu}\frac{dp}{dx}\left[y^2 - h^2\right] + \frac{U_w}{2}\left[\frac{y}{h} + 1\right], \tag{8}$$

where h is the channel half height and the co-ordinate system is based on that of Fig. 1. It can be shown that equation 8 is simply a linear combination of the expressions for the purely pressure-driven and purely wall-driven flows (a consequence of the “fully developed” nature of the flow

such that equation 5 becomes linear). For Poiseuille flow in a square duct, the following analytical solution [25] holds

$$u = U_b \frac{48}{\pi^3} \frac{\sum\limits_{i=1,3,5,\ldots}^{\infty} (-1)^{(i-1)/2} \left[1 - \frac{\cosh(i\pi y/2a)}{\cosh(i\pi b/2a)}\right] \frac{\cos(i\pi z/2a)}{i^3}}{1 - \frac{192a}{\pi^5 b} \sum\limits_{i=1,3,5,\ldots}^{\infty} \frac{\tanh(i\pi b/2a)}{i^5}}, \tag{9}$$

where a and b are as indicated in Fig. 2. Similarly, for the purely wall-driven flow with a single moving wall, the analytical solution [26] is

$$u = U_w \left(\frac{1-z}{2} + \sum_{n=1}^{\infty} \frac{2(-1)^n}{n\pi} . \sin\left[\frac{n\pi}{2}(1-z)\right] . \frac{\cosh(n\pi y/2)}{\cosh(n\pi/2)} \right). \tag{10}$$

The Couette-Poiseuille equation is then a linear combination of equation 9 and 10; simulation results from ANSYS Fluent are in excellent agreement with the resulting analytical solution for the fully-developed flow (see Fig. 3).

Mesh Independence Studies

To select a suitable mesh for the numerical simulations, a series of computations were carried out at $Re = 0.5$, 1 and 100, using different grids. For the 2D case, three structured cartesian meshes (M1, M2 and M3) were examined both for Poiseuille ($r = 0$) and Couette-Poiseuille flow with $r = 1$.

The accuracy of the fully developed profiles obtained from the simulations was estimated from the relative error

$$E = \left| \frac{u_{max} - u_{max,a}}{u_{max,a}} \right| \times 100, \tag{11}$$

where $u_{max,a}$ is the fully developed analytical value of the maximum streamwise velocity. The error (e) in the development length estimates (L_{Fluent}) from the meshes was also determined from

$$e = \left| \frac{L_{Fluent} - L_{extrap}}{L_{extrap}} \right| \times 100, \tag{12}$$

where L_{extrap} is the development length obtained from a Richardson extrapolation [24] of the results, and provides an estimate of the development length which is more accurate than the solution from the finest grid, M3. By fitting the values of E to an equation of the form $E = (\Delta x)^p + c$, the accuracy, p, of the numerical scheme was estimated to be second order (i.e. $p = 2$). This value of p was used in computing the Richardson extrapolations.

Results of the grid independence study in the 2D channel are summarised in Tab. 1. It can be observed that in meshes M2 and M3, the error values are small (E is less than 0.08%, while e is smaller than 0.7%). Since the difference in the value of L/D obtained from both meshes is less than 0.5%, all other simulations were conducted on grid M2.

For simulations in a square duct, six different meshes were tested (see Tab. 2). In all the grids, E is less than 0.4%, indicating that the fully developed flow fields from the simulations are highly accurate. However, for grids M1, M2, M3 and M4, all uniform meshes, the error in the development length estimates are large ($e = 10.58\%$ in the finest uniform mesh, M4). In M4, the total number of cells required for the simulation at $Re_D = 1$ was about twelve million, hence the computational cost, in terms of memory requirement and simulation time was very high. Therefore, a further refinement was not feasible, given the limited computational resources available. Instead, non-uniform meshes, M5 and M6 were tested. These grids are symmetrically stretched in the cross-sectional plane of the duct, such that the size of the maximum grid cell at the centre is four times larger than the smallest grid at the wall. Uniform streamwise spacing is employed in the moving-wall section, with the number of cells given by $N_x = N_y.L_w/D$ (where L_w is the length of the moving wall). Twenty grid cells, each, were employed in the two regions with stationary top walls (see Fig. 2b), the spacing increasing with distance from the moving wall. In mesh M6, e is less

than 1.5%. Since the simulations at higher Reynolds numbers required longer domains, hence larger number of grid cells, this mesh was used for subsequent computations as it allowed for a good compromise between accuracy and computational cost.

Development Length Computations in a 2D Channel

Figures 4a and b show the variation of development length with Reynolds number for Couette-Poiseuille flows in a 2D channel with uniform and parabolic inlet velocity profiles, respectively. The results cover wall to bulk velocity ratios spanning from zero (purely pressure-driven) to two (purely wall-driven). Here, the definition of L based on u_{max} location is employed, except for the purely wall-driven case where the global entry length is computed.

For purely pressure-driven flow with uniform inlet velocity, the results are in good agreement with the correlation of Durst *et al.* [1]. An increase in development length with r can be observed, thus indicating that longer ducts are required for fully developed wall-driven flows. In the creeping flow regime ($Re \to 0$), where diffusion dominates, L is essentially constant, and its value is of the order of the channel height, irrespective of the inlet boundary condition. For the case with parabolic inlet velocity profile at $r = 2/3$, it so happens that at the u_{max} location, the fully-developed velocity is close to the value at the inlet, hence a drop in L/D in the low Reynolds number regime can be observed. This effect appears to be less significant at high Reynolds numbers. In all the cases considered, L/D increases linearly with Re for $Re > 50$, while a non-linear behaviour can be observed in the region $2 < Re < 50$, consistent with the findings of [1], [6] and [4].

As shown earlier, the problem setup for the data of Fig. 4b is such that the moving wall is situated between two stationary walls, hence a further developing region is expected before the end of the translating wall is reached. Here, the velocity profile gradually changes to match the conditions in the stationary-wall region downstream. As this requires information to be propagated in the upstream direction, the process is dominated by molecular diffusion, and as expected, this development length was found to be of order D.

Estimates of L using the global entry length criteria were also obtained in this study. The plots follow the same trend as Figs. 4a and b hence they are not presented here. However, in Fig. 5a, the percentage difference in the entry length estimates from both definitions for $Re > 50$ is given

for the cases with parabolic inlet velocity profiles. It can be observed that the u_{max} criteria results in an under-prediction of L, hence for subsequent analyses, the global entry length criteria is used. In Fig. 5b, the effect of inlet boundary condition on the development length (also for $Re > 50$) is shown. The L values for flows developing from uniform and parabolic velocity profiles at the inlet can be observed to become increasingly the same as the ratio of wall to bulk velocity is increased. This indicates that the cross-stream diffusion transport becomes less important as r gets higher. However, there continues to remain a finite difference in the L estimates for flows with different inlet boundary conditions even in the limiting case of purely wall-driven flow (about 7%), hence diffusion cannot be totally neglected.

An attempt to collapse the L versus Re data at different r values onto a single plot was unsuccessful. Unfortunately, the only length scale present in this problem is the channel height, D. Normalising the development length by the half-height merely caused the entire data to be scaled by a factor of two in the vertical axis. Similarly, expressing the Reynolds number in terms of u_{max} or centreline velocity, did not yield a collapse. This is also the case for the 3D results which will be discussed later. In obtaining suitable correlations for the development length, we adopt a pragmatic approach. For $Re < 1$, a reasonable estimate of the entry length for practical applications can be obtained by taking L to be $\mathcal{O}(D)$. For $Re > 50$, we compute the value of the coefficient C_1 in equation 1 at all wall-to-bulk velocity ratios considered. The results are plotted in Figs. 6a and b. The data are well fit ($R^2 = 0.9995$ and 0.9978 respectively) by the following power-law relations for the cases with uniform and parabolic inlet velocity profiles respectively:

$$C_1 = 0.04484 + 0.04123r^{1.27} \tag{13}$$

$$C_1 = 0.06167r^{1.123}, \tag{14}$$

hence accurate predictions of L at high Reynolds numbers can be made by simply using the

expression $L/D = C_1 Re$. For the case with uniform inlet velocity, C_1 reduces to the value given by [1] at $r = 0$. Similarly, for parabolic inlet velocity, the curve of Fig. 6b extrapolates to zero at $r = 0$ as expected.

Development Length Computations in a Square Duct

For an investigation of the entry length requirements in a 3D flow, we consider a duct of square cross-section. In computing L for this case, the velocity profiles along the vertical and horizontal wall-bisectors were examined. In the purely pressure-driven flow with a uniform inlet velocity profile, the development length can be observed to be greater than in a 2D channel (see Fig. 7, where the correlation of [1] for channel and pipe flow are included), hence 3D effects introduced by the side walls cannot be neglected.

The L/D estimates in the square duct are much closer to those in the pipe. A possible reason for the observed difference is the non-uniform distribution of the wall shear stress in the former, especially, close to the corners. It is therefore expected that similar results will be obtained in both geometries if the square duct corners are rounded. A better collapse in the correlations of [1] for pipes and 2D channels can be observed when the Reynolds number is expressed in terms of the centreline velocity, U_c (see inset of Fig. 7), but L/D is still slightly higher in the duct (with a maximum difference of about 20%).

Figure 8a shows the variation of development length in a square duct with Re for r ranging from $2/3$ to 4 (purely wall-driven flow; unlike in the 2D channel, U_b=$U_w/4$ in this case, where U_w is the wall velocity, therefore, $U_w/U_b = r = 4$). Here, a parabolic velocity profile is imposed at the inlet. As a result of the computational difficulties discussed earlier, only a limited number of simulations were conducted at $Re > 10$. The development length can be observed to become larger with increasing r, similar to the observations in the 2D channel. Figure 8b shows the variation of L with r in the limit as $Re \to 0$. As expected, L is higher in ducts with uniform inlet velocity profiles.

The data is fairly well fitted ($R^2 = 0.985$) by a linear curve: $L/D = C_0 = 0.1366r + 0.7673$. For the simulations with parabolic inlet velocities, a line with the same slope, but a smaller intercept (0.49), fits well to the data in the region $0.5 < r < 4$. It should be noted that the development length in the limiting case of purely pressure-driven flow (i.e. $r = 0$) must be equal to zero, as a

result of the inlet boundary condition, hence it is not surprising that there is a non-linear behaviour in the region, $r < 0.5$. In Fig. 8a, the data points at $Re > 10$ appear to diverge after being roughly parallel in the creeping-flow regime, hence values of the slope, C_1, in the $Re \to \infty$ limit cannot be inferred from the plots in Fig. 8b. For $r = 2/3$, where numerical data up to $Re = 200$ has been obtained, a linear fit to the data points indicates that $C_1 \approx 0.0477$ in the high Reynolds number limit.

EXPERIMENTAL STUDIES

In an effort to investigate the effect of wall motion on the laminar flow fields in ducts, a new test-section for examining these flows was designed and constructed at the Fluids Engineering laboratory in the University of Liverpool. This section was incorporated into the square duct rig described in [27]. The numerical simulation data previously presented were used as a guide in deciding on the dimensions of the facility. Here, we present the results of the detailed tests conducted to determine the laminar flow entry length requirements and thus provide validation for the square duct simulations. The new rig can also be used for turbulent flow investigations; however, as the focus of this paper is on laminar flows, these are not included. Figure 9 shows the Couette-Poiseille flow test-section. Translatory motion is implemented using an endless stainless steel belt driven by three pulleys, one of which is connected to an electric motor. This arrangement results in a moving wall of length $6.25D$. The experimental setup matches the configuration of Fig. 2b. The test-section is enclosed in a casing made of PVC plastic, which contains the working fluid, and glass windows are provided to allow for optical access to the flow for laser Doppler velocimetry (LDV) measurements. The entire square duct rig consists of nine additional stainless steel modules (eight modules before the moving-wall section and one after), each having a length of 1.2 m and cross-sectional dimensions 80 mm $\times$ 80 mm. Transition sections designed to vary in cross-section from circular to square or vice versa are also introduced at the inlet and outlet of the duct to ensure smoothly varying flow.

The Poiseuille component was generated by pumping fluid through the duct at different flow rates. To these pressure-driven flows, a Couette component was introduced by translating the

stainless steel belt. In all the measurements, the wall moves in the same direction as the bulk flow and Glycerol/water solution (70/30% by volume) with an Ekman number of about 12 was employed as working fluid. The results of laminar flow simulations at $Ek = 12$ (Coriolis body force included) are identical to those in which no body forces are included; hence Coriolis effects [27, 28] are negligible at this Ekman number.

Figures 10a and b show the velocity data at different distances from the inlet in Couette-Poiseuille flows with $r = 1.7$ and 1 and $Re = 67$ and 76, respectively. The measurement locations ($y/D = 0.3$ and 1, respectively) correspond to positions of maximum streamwise velocity in the analytical solution. The uncertainty in the LDV data is estimated to be about 3% (as indicated by the error bars), hence, the criteria that the velocity profile be within 1% of the laminar analytical solution is rather stringent. This explains why an accurate experimental determination of L has so far been unsuccessful [1]. In Fig. 10a ($r \approx 1.7$), an increase in the measured velocity with increasing streamwise distance can be observed, with a plateau region occurring at about $x/D \gtrsim 4$. However, in all but the first data point, the analytical solution is within the error bounds of the measurements.

For $r \approx 1$ (Fig. 10b), it appears that the flow is already fully-developed at the first measurement location accessible by the LDV probe ($x/D \approx 2.35$). This is consistent with the simulation results (see Fig. 8).

From the afore-reported measurements, it is clear that at the Reynolds numbers considered, fully-developed flows can be obtained at $x/D \approx 4.69$ (the furthest downstream position accessible by the LDV probe). Figure 11 shows the velocity profiles at this location. Measurements of the developing profile at $x/D \approx 2.5$ and $r \approx 1.7$ are also included. The agreement with the analytical solution as well as numerical simulation resullts from ANSYS Fluent is striking. To the best of the authors' knowledge, this is the first time such measurements are reported.

CONCLUSIONS

The results of numerical simulations and experiments conducted to determine the develoment/entry lengths (L) in laminar Couette-Poiseuille flows through a 2D channel and a 3D square

duct have been presented. The development lengths were observed to be higher than those in purely pressure-driven flows, L becoming larger as the wall-to-bulk velocity ratio is increased. An attempt to collapse the data onto a single curve, using various velocity and length scales, was not successful. However, suitable correlations for predicting L in the low and high Reynolds number limits have been developed. Consistent with the findings of Durst *et al.* [1], L was observed to be essentially constant, and of the order of the channel height, D, in the creeping-flow regime (i.e. as $Re \to 0$). However, for $Re \gtrsim 50$, the development length increased linearly with Reynolds number. The inlet boundary condition was found to be important, as L was observed to be higher in flows with uniform velocity profiles at the inlet than those with parabolic velocity profiles. However, the entry length estimates obtained from both inlet conditions were found to be increasingly similar as the purely wall-driven flow limit is approached. LDV measurements in a test section designed to investigate these flows indicate that fully-developed flow fields can be obtained at the Reynolds numbers tested. The experimental data in the fully-developed region at $r = 1.7$ and 1 agree well with the laminar analytical solution. Measurements in the developing region are also in good agreement with the numerical simulation results.

REFERENCES

[1] Durst, F., Ray, S., Ünsal, B., and Bayoumi, O., 2005. "The development lengths of laminar pipe and channel flows". *ASME J. Fluids Eng.,* **127**(6), pp. 1154–1160.

[2] Shah, R. K., and London, A. L., 1978. *Laminar flow forced convection in ducts: a source book for compact heat exchanger analytical data*. Academic press.

[3] McComas, S., 1967. "Hydrodynamic entrance lengths for ducts of arbitrary cross section". *ASME J. Basic Eng.,* **89**(4), pp. 847–850.

[4] Poole, R. J., 2010. "Development-length requirements for fully developed laminar flow in concentric annuli". *ASME J. Fluids Eng.,* **132**(6), p. 064501.

[5] Poole, R. J., and Chhabra, R. P., 2010. "Development length requirements for fully developed laminar pipe flow of yield stress fluids". *ASME J. Fluids Eng.,* **132**(3), p. 034501.

[6] Poole, R. J., and Ridley, B. S., 2007. "Development-length requirements for fully developed laminar pipe flow of inelastic non-Newtonian liquids". *ASME J. Fluids Eng.,* **129**(10), pp. 1281–1287.

[7] Joshi, Y., and Vinoth, B. R., 2018. "Entry lengths of laminar pipe and channel flows". *ASME J. Fluids Eng.,* **140**(6), p. 061203.

[8] Yunus, A. C., and Cimbala, J. M., 2006. "Fluid mechanics fundamentals and applications". *McGraw-Hill*.

[9] Tatsumi, T., and Yoshimura, T., 1990. "Stability of the laminar flow in a rectangular duct". *J. Fluid Mech.,* **212**, pp. 437–449.

[10] Kountouriotis, Z., Philippou, M., and Georgiou, G. C., 2016. "Development lengths in newtonian poiseuille flows with wall slip". *Appl. Maths. Comp.,* **291**, pp. 98–114.

[11] Philippou, M., Kountouriotis, Z., and Georgiou, G. C., 2016. "Viscoplastic flow development in tubes and channels with wall slip". *J. non-Newtonian Fluid Mech.,* **234**, pp. 69–81.

[12] Ferrás, L., Afonso, A., Alves, M., Nóbrega, J., and Pinho, F., 2012. "Development length in planar channel flows of newtonian fluids under the influence of wall slip". *ASME J. Fluids Eng.,* **134**(10), p. 104503.

[13] Galvis, E., Yarusevych, S., and Culham, J., 2012. "Incompressible laminar developing flow in

microchannels". *ASME J. Fluids Eng.,* **134**(1), p. 014503.

[14] Ray, S., Ünsal, B., and Durst, F., 2012. "Development length of sinusoidally pulsating laminar pipe flows in moderate and high reynolds number regimes". *Int. J. Heat Fluid Flow,* **37**, pp. 167–176.

[15] Muzychka, Y., and Yovanovich, M., 2009. "Pressure drop in laminar developing flow in non-circular ducts: A scaling and modeling approach". *ASME J. Fluids Eng.,* **131**(11), p. 111105.

[16] Astill, K. N., Ganley, J. T., and Martin, B. W., 1968. "The developing tangential velocity profile for axial flow in an annulus with a rotating inner cylinder". *Proc. Roy. Soc. Lond.,* **307**(1488), pp. 55–69.

[17] Holeschovsky, U. B., and Cooney, C. L., 1991. "Quantitative description of ultrafiltration in a rotating filtration device". *AIChE J.,* **37**(8), pp. 1219–1226.

[18] Cohen, S., and Marom, D. M., 1983. "Experimental and theoretical study of a rotating annular flow reactor". *Chem. Eng. J.,* **27**(2), pp. 87–97.

[19] Dennis, D. J. C., Seraudie, C., and Poole, R. J., 2014. "Controlling vortex breakdown in swirling pipe flows: experiments and simulations". *Phys. Fluids,* **26**(5), p. 053602.

[20] Mettu, S., Verma, N., and Chhabra, R., 2006. "Momentum and heat transfer from an asymmetrically confined circular cylinder in a plane channel". *Heat and Mass Transfer,* **42**(11), pp. 1037–1048.

[21] Chakraborty, J., Verma, N., and Chhabra, R., 2004. "Wall effects in flow past a circular cylinder in a plane channel: a numerical study". *Chem. Eng. Proc.,* **43**(12), pp. 1529–1537.

[22] Escudier, M. P., OLeary, J., and Poole, R. J., 2007. "Flow produced in a conical container by a rotating endwall". *Int. J. Heat Fluid Flow,* **28**(6), pp. 1418–1428.

[23] Fellouah, H., Castelain, C., El Moctar, A., and Peerhossaini, H., 2006. "A numerical study of dean instability in non-newtonian fluids". *ASME J. Fluids Eng.,* **128**(1), pp. 34–41.

[24] Ferziger, J. H., and Peric, M., 2012. *Computational methods for fluid dynamics*, 3rd ed. Springer Science & Business Media, London.

[25] White, F. M., 2006. *Viscous fluid flow*, 3rd ed. McGraw-Hill, New York.

[26] Davoodi, M., Lerouge, S., Norouzi, M., and Poole, R. J., 2018. "Secondary flows due to finite

aspect ratio in inertialess viscoelastic Taylor-Couette flow". *J. Fluid Mech.,* **857**, pp. 823–850.

[27] Owolabi, B. E., Poole, R. J., and Dennis, D. J. C., 2016. "Experiments on low-Reynolds-number turbulent flow through a square duct". *J. Fluid Mech.,* **798**, pp. 398–410.

[28] Draad, A., and Nieuwstadt, F., 1998. "The earth's rotation and laminar pipe flow". *J. Fluid Mech.,* **361**, pp. 297–308.

LIST OF FIGURES

10 Couette-Poiseuille flow development. (a) $r \approx 1.7$ and $Re \approx 63$. (b) $r \approx 1$ and $Re \approx 76$. Measurements have been taken at $y/D = 0.3$ in (a) and $y/D = 0.1$ in (b) along the vertical wall bisector, corresponding to the respective maximum velocity locations. Error bars representing $\pm 3\%$ measurement uncertainty have been included.

11 Velocity profiles in laminar Couette-Poiseuille flows in a square duct: (a) fully-developed profiles along the wall bisectors at $x/D \approx 4.69$, $Re \approx 63$ and $r \approx 1.7$; (b) fully-developed profile taken at the same streamwise location and Re as (a) at $y/D = 0.375$ (10 mm from moving wall); (c) velocity profiles along the wall bisectors in developing flow at $x/D \approx 2.5$, $Re \approx 63$ and $r \approx 1.7$; (d) fully-developed profiles at $x/D \approx 4.69$, $Re \approx 76$ and $r \approx 1$. Unfilled symbols represent profiles along the vertical plane (from the bottom stationary wall to the top moving wall), while filled symbols represent those along the horizontal plane (from one stationary side wall to the other). Solid lines represent the laminar flow analytical solution for fully-developed flow, while dash-dotted lines represent the developing flow numerical simulation results from ANSYS Fluent.

LIST OF TABLES

FIGURES

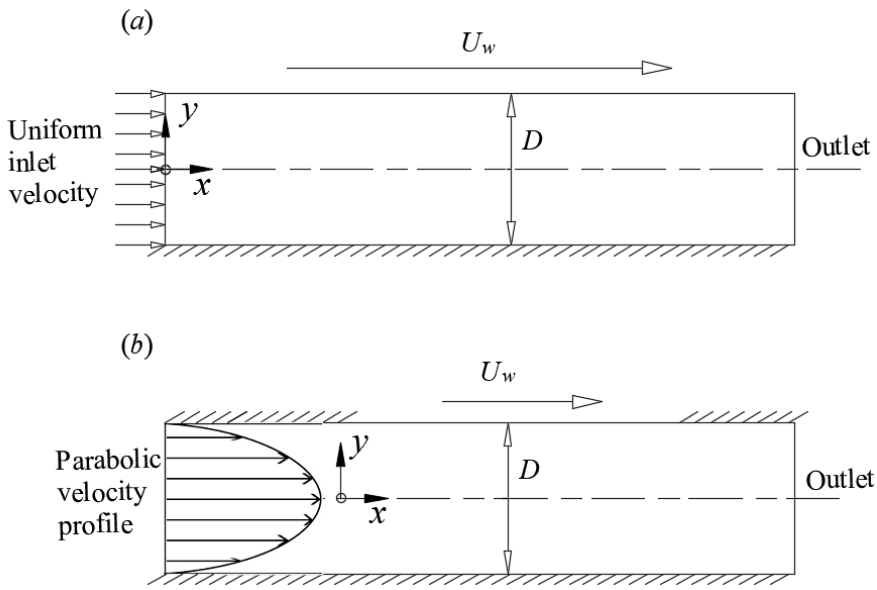

Fig. 1. Computational domain and boundary conditions for the flow in a 2-D channel: (a) uniform inlet velocity, (b) parabolic velocity profile at the inlet.

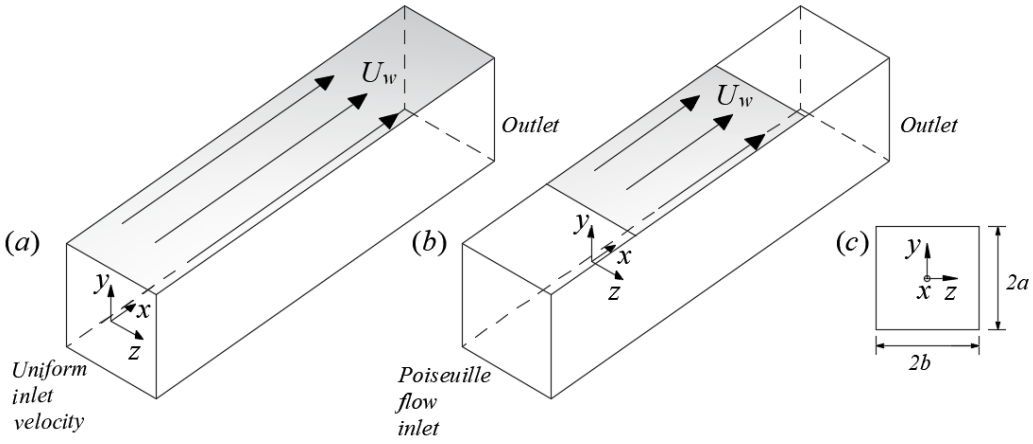

Fig. 2. Computational domain and boundary conditions for the flow in a square duct: (a) uniform inlet velocity, (b) parabolic velocity profile at the inlet. Moving wall is shaded.

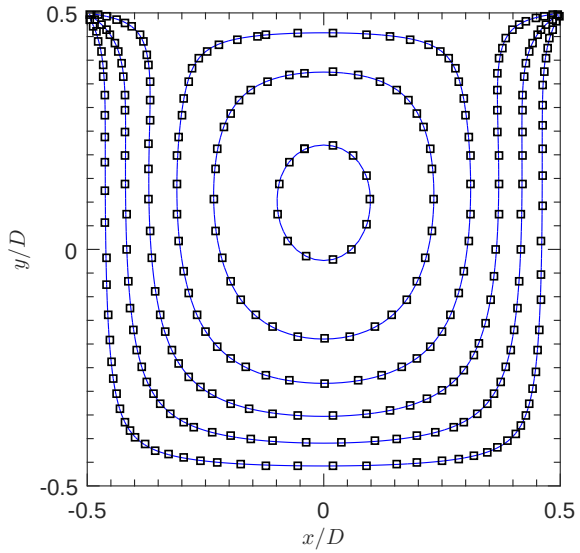

Fig. 3. Comparison between u/U_b from analytical solution and numerical simulation at $r = 1$. Symbols represent numerical simulation while lines represent the analytical solution. Values of u/U_b shown, range from 0.3 to 1.8 with increment of 0.3. Translatory motion is introduced at the top wall.

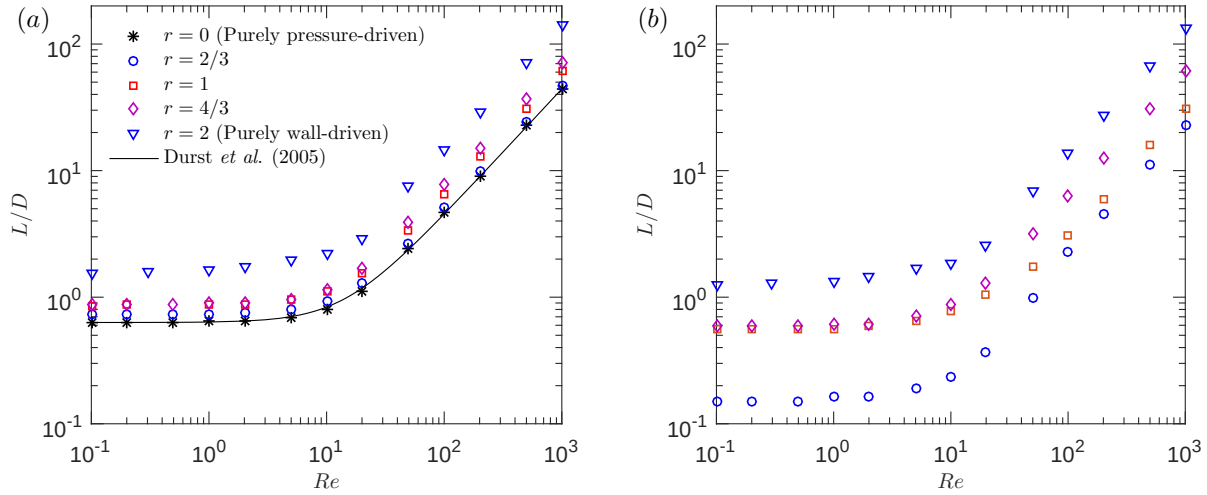

Fig. 4. Development lengths in a 2D channel at different wall to bulk velocity ratios: (a) Uniform inlet velocity. (b) Parabolic velocity profile at the inlet. L is the entry length at the wall-normal location corresponding to u_{max}.

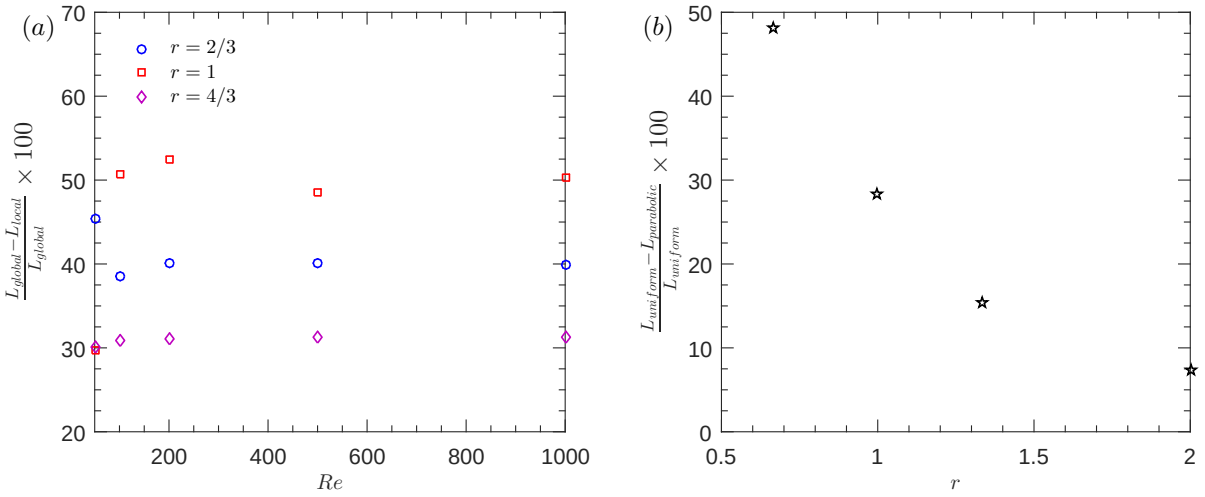

Fig. 5. Development length computations in a 2D channel at high Reynolds numbers: (a) Influence of entry length definition. (b) Effect of inlet boundary condition. L_{global} is the global entry length while L_{local} is the development length computed at the wall-normal location corresponding to u_{max}. Plots show results at $Re > 50$.

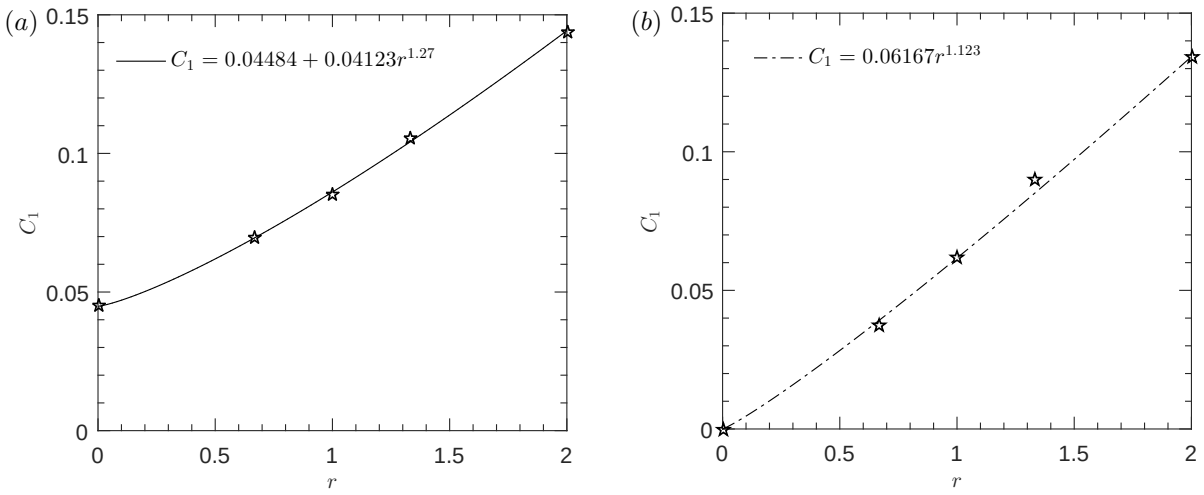

Fig. 6. Correlations for C_1: (a) Uniform inlet velocity. (b) Parabolic velocity profile at the inlet

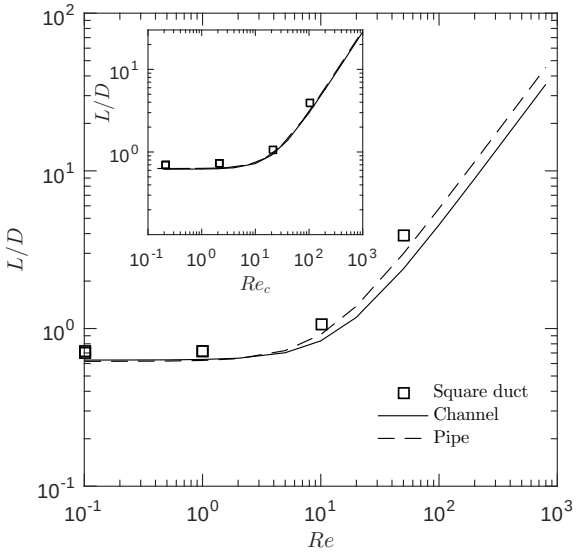

Fig. 7. Development lengths in purely pressure-driven flows. Inset shows better collapse when centreline velocity scaling is used to define Re ($Re_c = \rho U_c D/\mu$).

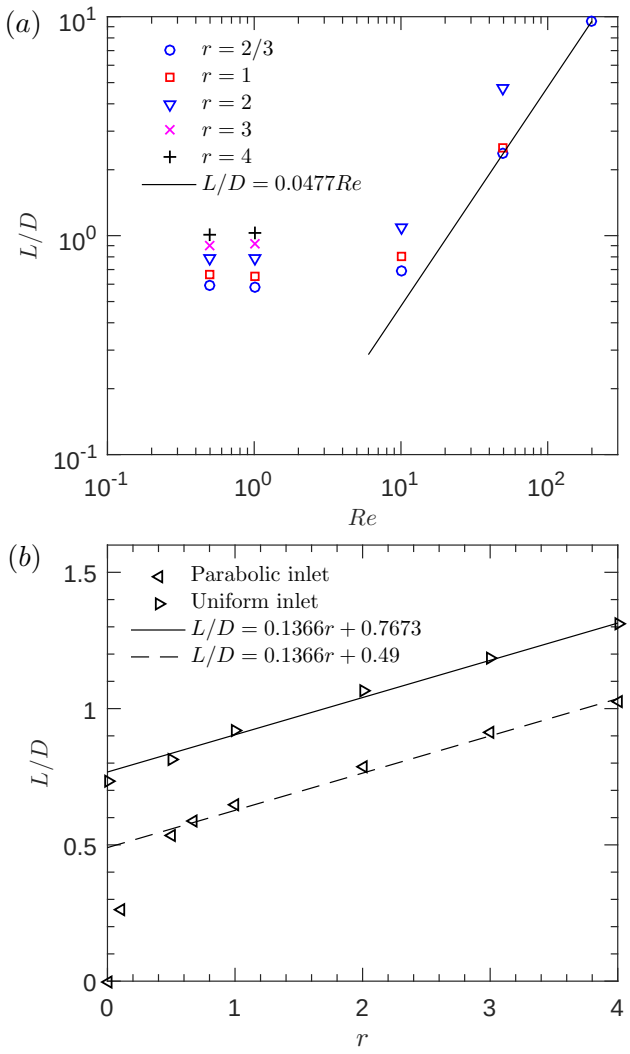

Fig. 8. Couette-Poiseuille flow development length simulations in a square duct: (a) Development lengths at Re ranging from 0.5 to 200 for parabolic velocity profile at the inlet. (b) Development lengths at $Re \to 0$.

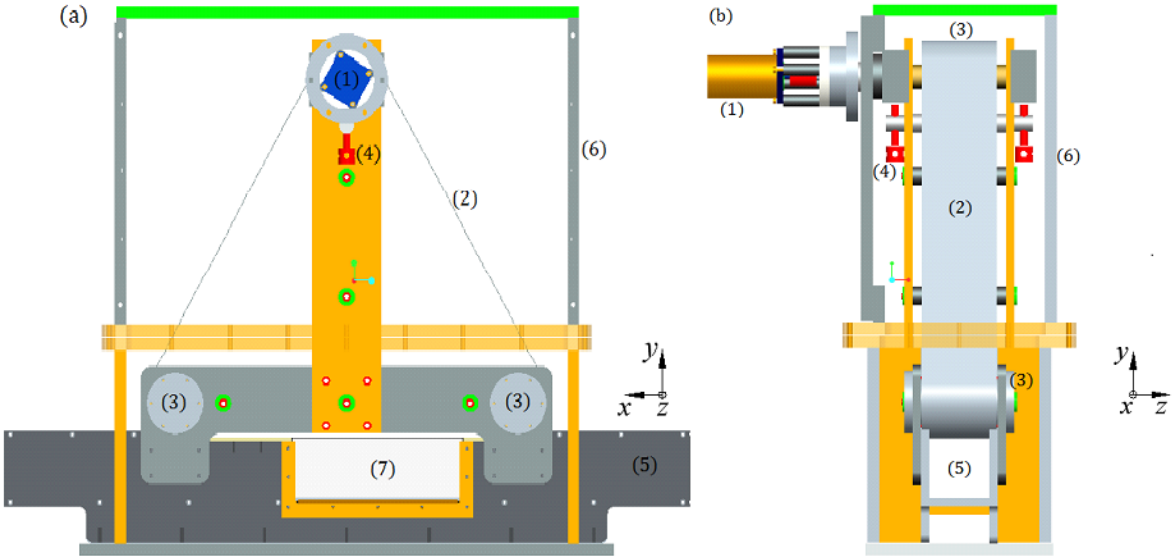

Fig. 9. Experimental test section for the study of wall-driven flows: (a) Side view. (b) Front view. (1) electric motor; (2) stainless steel belt; (3) pulleys; (4) tracking screw; (5) square duct; (6) water-tight casing; (7) borosilicate glass window. Flow is in the positive x direction.

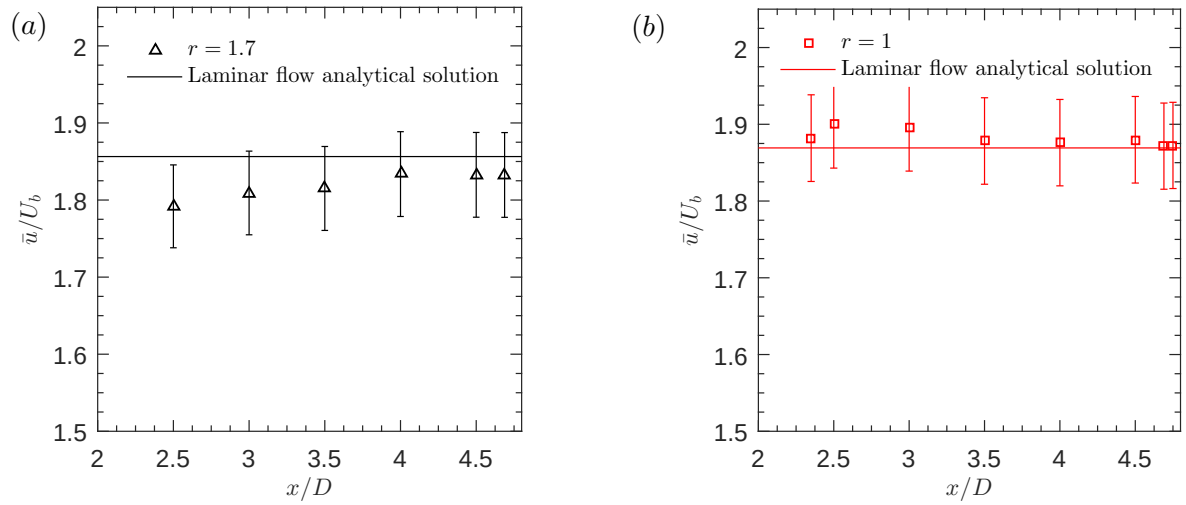

Fig. 10. Couette-Poiseuille flow development. (a) $r \approx 1.7$ and $Re \approx 63$. (b) $r \approx 1$ and $Re \approx 76$. Measurements have been taken at $y/D = 0.3$ in (a) and $y/D = 0.1$ in (b) along the vertical wall bisector, corresponding to the respective maximum velocity locations. Error bars representing $\pm 3\%$ measurement uncertainty have been included.

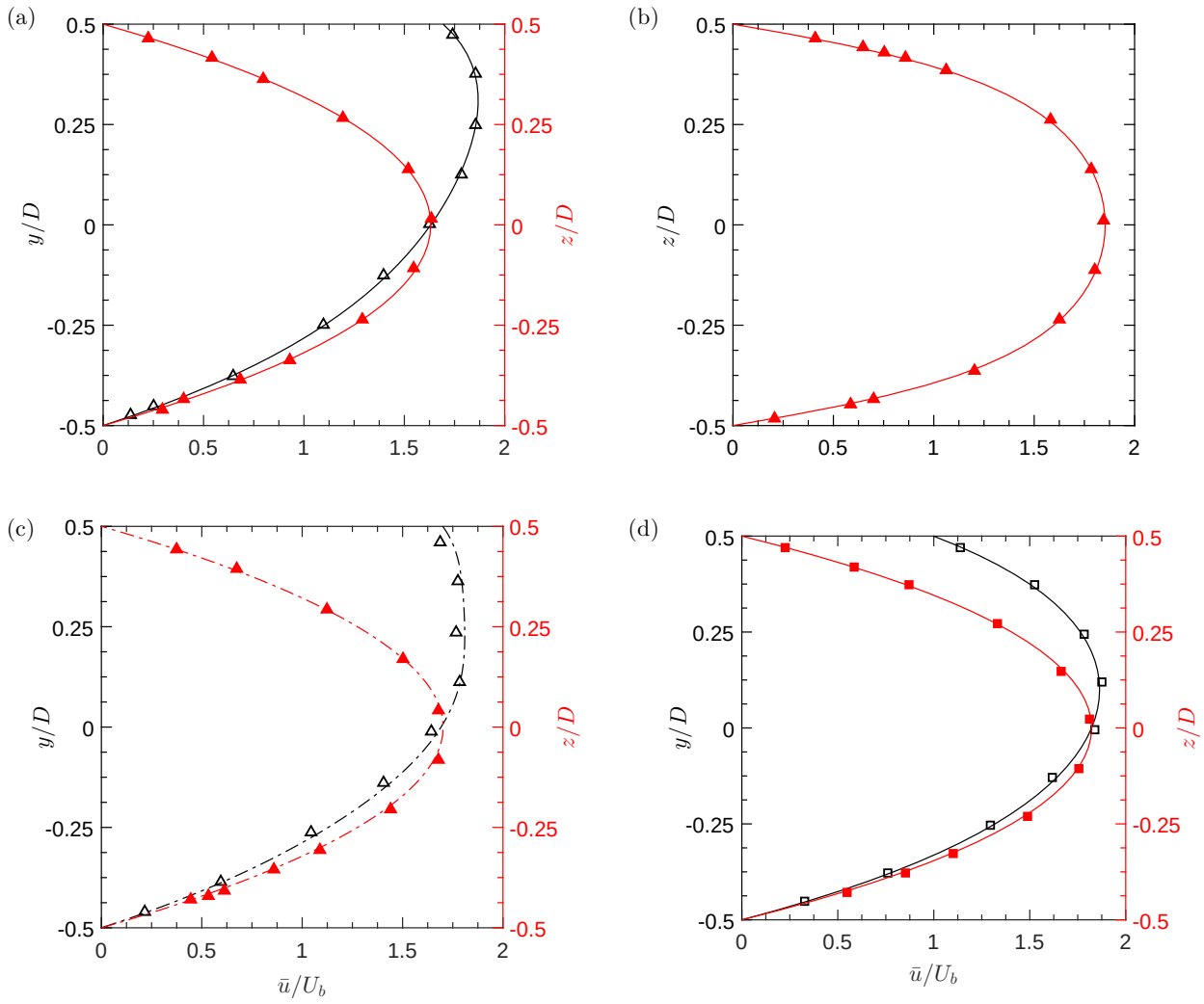

Fig. 11. Velocity profiles in laminar Couette-Poiseuille flows in a square duct: (a) fully-developed profiles along the wall bisectors at $x/D \approx 4.69$, $Re \approx 63$ and $r \approx 1.7$; (b) fully-developed profile taken at the same streamwise location and Re as (a) at $y/D = 0.375$ (10 mm from moving wall); (c) velocity profiles along the wall bisectors in developing flow at $x/D \approx 2.5$, $Re \approx 63$ and $r \approx 1.7$; (d) fully-developed profiles at $x/D \approx 4.69$, $Re \approx 76$ and $r \approx 1$. Unfilled symbols represent profiles along the vertical plane (from the bottom stationary wall to the top moving wall), while filled symbols represent those along the horizontal plane (from one stationary side wall to the other). Solid lines represent the laminar flow analytical solution for fully-developed flow, while dash-dotted lines represent the developing flow numerical simulation results from ANSYS Fluent.

TABLES

Table 1. Grid independence study for Couette-Poiseuille flow in a two-dimensional channel with uniform inlet velocity profile. N_y and N_x are the number of cells in the wall-normal and streamwise directions respectively, while L_w is the length of the moving wall.

Mesh	$N_y \times N_x$	$\Delta x/D = \Delta y/D$	u_{max}/U_b	$E(\%)$	L/D	$e(\%)$
$r = 0$ (purely pressure-driven flow), $Re = 0.5$						
M1	$40 \times 40 L_w/D$	0.025	1.49496	0.274	0.650	2.52
M2	$80 \times 80 L_w/D$	0.0125	1.49953	0.072	0.638	0.63
M3	$160 \times 160 L_w/D$	0.00625	1.49988	0.019	0.635	0.16
Richardson extrapolation					0.634	
$r = 0$, $Re = 100$						
M1	$40 \times 40 L_w/D$	0.025	1.49792	0.139	4.865	3.53
M2	$80 \times 80 L_w/D$	0.0125	1.49942	0.039	4.723	0.51
M3	$160 \times 160 L_w/D$	0.00625	1.49984	0.011	4.705	0.13
Richardson extrapolation					4.699	
$r = 1$, $Re = 0.5$						
M1	$40 \times 40 L_w/D$	0.025	1.33208	0.132	0.877	1.50
M2	$80 \times 80 L_w/D$	0.0125	1.33302	0.034	0.867	0.35
M3	$160 \times 160 L_w/D$	0.00625	1.33325	0.006	0.865	0.12
Richardson extrapolation					0.864	

Table 2. Grid independence study for Couette-Poiseuille flow in a square duct at $Re = 1$ and $r = 2/3$. Inlet velocity profile is parabolic.

Mesh	$N_y \times N_x$	$\Delta y/D = \Delta z/D$	u_{max}/U_b	$E(\%)$	L/D	$e(\%)$
		Uniform mesh				
M1	$50 \times 50 \times 50 L_w/D$	0.0200	1.92086	0.370	0.84	55.84
M2	$60 \times 60 \times 60 L_w/D$	0.0167	1.92266	0.277	0.783	45.27
M3	$100 \times 100 \times 100 L_w/D$	0.0100	1.92626	0.090	0.62	15.03
M4	$120 \times 120 \times 120 L_w/D$	0.0083	1.92630	0.088	0.596	10.58
Richardson extrapolation					0.539	
		Non-uniform mesh				
M5	$90 \times 90 \times (90 L_w/D + 40)$		1.92446	0.184	0.556	3.15
M6	$95 \times 95 \times (95 L_w/D + 40)$		1.92582	0.114	0.547	1.48